

# Statistical Mechanics of DNA Rupture: Theory and Simulations

S. Nath, T. Modi<sup>1</sup>, R. K. Mishra, D. Giri<sup>1</sup>, B. P. Mandal and S. Kumar

*Department of Physics, Banaras Hindu University, Varanasi 221 005, India*

<sup>1</sup> *Department of Physics, Indian Institute of Technology (BHU), Varanasi 221005, India*

## Abstract

We study the effects of the shear force on the rupture mechanism on a double stranded DNA. Motivated by recent experiments, we perform the atomistic simulations with explicit solvent to obtain the distributions of extension in hydrogen and covalent bonds below the rupture force. We obtain a significant difference between the atomistic simulations and the existing results in the literature based on the coarse-grained models (theory and simulations). We discuss the possible reasons and improve the coarse-grained model by incorporating the consequences of semi-microscopic details of the nucleotides in its description. The distributions obtained by the modified model (simulations and theoretical) are qualitatively similar to the one obtained using atomistic simulations.

PACS numbers:

## I. INTRODUCTION

Single molecule force spectroscopy (SMFS) techniques have enhanced our understanding about the inter- and intra- molecular interactions involved in the stability of DNA and biological processes *e.g.* transcription, replication, slippage, rupture etc. [1–13]. Initially, it was thought that the interactions detected in SMFS experiments would be mostly of a mechanical nature and can be calculated by knowing the value of the applied force. However, insights gathered from these experiments revealed that the measurement of molecular interactions depends not only on the magnitude of the applied force, but also on how and where the force is applied [3–13]. For example, Bockelmamm and coworkers [4, 5] applied the force perpendicular to the helix direction (DNA unzipping) and measured the unzipping force  $\sim 15$  pN, whereas, Lee et al [6] studied the unbinding of double stranded DNA (dsDNA) by applying a force along the helix direction (rupture of DNA), and measured the rupture force, which is one order magnitude greater than the unzipping force. Strunz *et al* [7, 8] investigated the unbinding of DNA duplex of various lengths and found that the unbinding force depends on the loading rate and sequence length. It was also found that changing the pulling direction results different unbinding forces [11, 13].

By expressing the bond energy and base-pairing energy in the form of harmonic oscillators in the ladder model of dsDNA (homosequence) of length  $N$  base-pairs, de Gennes [14] proposed the maximum force required for the rupture is

$$F_c = 2f_1(\chi^{-1} \tanh(\chi \frac{N}{2})), \quad (1)$$

where  $f_1$  is the force required to separate a single base-pair and  $\chi^{-1} = \sqrt{Q/2R}$  is the de Gennes characteristic length. Here,  $Q$  and  $R$  are the spring constants of covalent (backbone) and hydrogen bonds, respectively. Eq. 1 predicts that the rupture force increases linearly with length for small values of  $N$  and saturates at the higher values of  $N$ , which is consistent with recent experiment [10]. In an another study, Chakrabarti and Nelson [15] extended the de Gennes model (nonlinear generalization of the ladder model) and studied the effects of sequence heterogeneity. Mishra *et al* [16] considered a homosequence of DNA, where the covalent bonds and base-pairing interactions are modeled by the harmonic spring and Lennard-Jones (LJ) potential, respectively. Using Langevin

dynamics (LD) simulations [17, 18], they obtained the distribution of stretching of hydrogen bonds and the extension in the covalent bonds for a wide range of forces below the rupture, which are experimentally difficult to obtain.

In this paper, we study the rupture event of the base sequence studied in the recent experiments [10]. In Sec. II, we discuss results from atomistic simulations with explicit solvent. We shall confine ourselves to a chain of 12 base-pairs only and focus on the following issues: (i) distribution of stretching of hydrogen bonds, and (ii) the extension in the covalent bonds along the strand. For the comparison, we also study a homosequence (A-T) of same length as studied in Ref. [16]. Though the distribution obtained here is qualitatively similar to the one obtained in Ref. [16], but showed the asymmetry in the distribution for the both cases. In Sec. III, we discuss the possible reason for this discrepancy. Since, the computational cost involved in the atomistic computation is very large and beyond our computational limit for a longer DNA, we consider a coarse-grained description of dsDNA to study the rupture events. We incorporate consequences arising due to the semi-microscopic details of nucleotides in the model to explain the asymmetry in the distributions. In order to substantiate our findings, we revisit the ladder model of DNA [14] in Sec. IV, and redefine the de Gennes characteristic length for a realistic chain to obtain the modified formula for the rupture force, which is in good agreement with the coarse-grained simulations. Analytical results developed here are consistent with the experiments and simulations. Finally, Sec. V concludes with a brief discussion.

## II. ATOMISTIC SIMULATIONS OF DNA RUPTURE

In order to have a better understanding of the rupture events, we perform atomistic simulations of experimental [10] sequence of length of 12 base-pairs with explicit solvent. More specifically, here, we are interested in the distribution of extension in the hydrogen and covalent bonds of dsDNA along the chain at the semi-microscopic level, which is otherwise difficult to obtain. We have used AMBER10 software package [19] with all atom (ff99SB) force field [20] to simulate the rupture event of DNA. A force routine has been added in AMBER10 to do simulation at constant force [21, 22]. In this case, the force has been applied at  $5' - 5'$  ends as shown in Fig.1. The

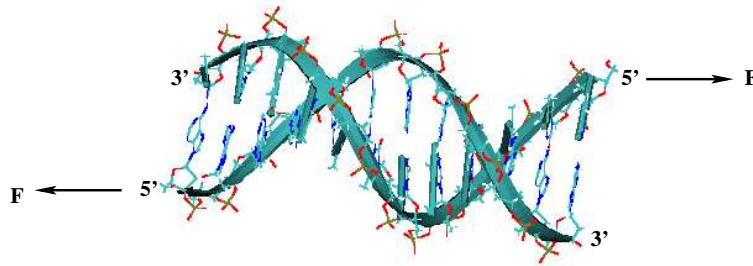


FIG. 1: Schematic representation of dsDNA under the shear force applied at 5' – 5' ends.

electrostatic interactions have been calculated with Particle Mesh Ewald (PME) method [23, 24] using a cubic B-spline interpolation of order 4 and a  $10^{-5}$  tolerance is set for the direct space sum cut off. A real space cut off of  $10 \text{ \AA}$  is used for both the van der Waal and the electrostatics interactions. The starting structure of the DNA duplex sequence (GTCACCTTAGAC) is built using the NAB module of the AMBER10 suit of programs. Using the LEaP module in AMBER, we add the  $Na^+$  (counterions) to neutralize the negative charges on phosphate backbone group of DNA structure. This neutralized DNA structure is immersed in water box using TIP3P model for water [25]. We have chosen the box dimension in such a way that the ruptured DNA structure remains fully inside the water box. For the 12 base-pairs sequence, we have taken the box size of  $55 \times 56 \times 199 \text{ \AA}^3$  which contains 16690 water molecules and 22  $Na^+$  (counterions). The system is equilibrated at  $F = 0$  for 100 ps under a protocol described in Ref. [26, 27]. We carried out simulations in the isothermal-isobaric (NPT) ensemble using a time step of 1 fs. We maintain the constant pressure by isotropic position scaling [19] with a reference pressure of 1 atm and a relaxation time of 2 ps. Constant temperature was maintained at 320 K using Langevin thermostat with a collision frequency of  $1 \text{ ps}^{-1}$ . We have used 3D periodic boundary conditions during the simulation.

To simulate the stretching of hydrogen bonds, we give sufficient time for equilibrium at constant force. The magnitude of the applied constant force is 570 pN for the 12 base-pairs, which is sufficient enough for separating the both strands of dsDNA. To have a better understanding,

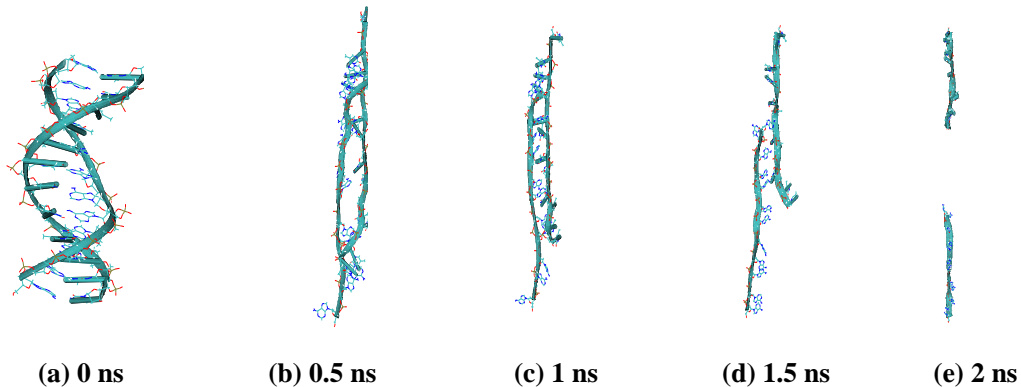


FIG. 2: Snapshots (generated using VMD software) of dsDNA ( $N = 12$ ) under constant shear force applied at  $5' - 5'$  ends, taken at different time: (a)  $0 \text{ ns}$ , (b)  $0.5 \text{ ns}$ , (c)  $1.0 \text{ ns}$ , (d)  $1.5 \text{ ns}$ , and (e)  $2.0 \text{ ns}$ . These snapshots show the rupture process at  $T = 320\text{K}$ . We have not shown water molecules and counterions in the snapshots for the clarity.

we have monitored the deformations in DNA at different instants of time. In Fig. 2, we have shown some of the snapshots of the conformation (generated by visual molecular dynamics (VMD) software [29] under constant shear force applied at  $5' - 5'$  ends at a temperature  $320 \text{ K}$ . Initially, the dsDNA remains in the zipped state as shown in Fig. 2 (a). As time passes, the dsDNA goes to a ladder form (Fig. 2(b)) and then complete rupture takes place (Fig. 2 (e)). Fig. 3a shows the variation of extension in hydrogen bond length ( $\Delta_h$ ) and covalent bond length ( $\Delta_c$ ) (i.e. deviation from their mean length) along the chain with base position. We have monitored the distance of  $C4'$  atom of complementary bases in dsDNA to measure the extension in hydrogen bond length. We have studied the system just before the rupture. Simulation results show the asymmetry in the distribution of stretching of hydrogen bond (Fig. 3a) and covalent bonds (Fig. 3b).

In order to see, whether this asymmetry is because of heterogeneity of the sequence, we have

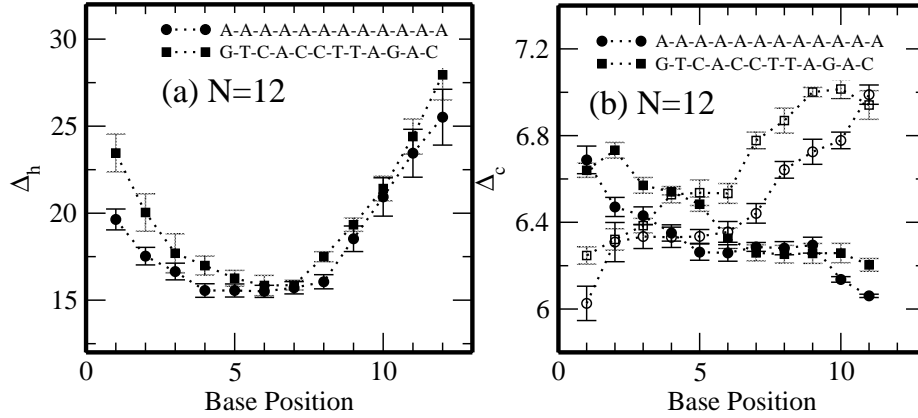


FIG. 3: Fig (a) shows the variation of extension in hydrogen bond length ( $\Delta_h$ ) along the chain with base position for the chain of 12 base-pairs of the designed and experimental sequence; (b) Same as Fig. a but for the extension in covalent bonds ( $\Delta_c$ ) along the chain length. Here, open and filled symbols correspond to one strand and its complementary strand, respectively. The dotted lines are guide to the eye.

repeated the simulation for a designed homosequence (AAAAAAAAAAAA) of the same length. The rupture force for this sequence is about 460 pN. It may be noted that the simulation carried out by Mishra et al [16] or the analytical solution proposed by de Gennes [14], showed that distribution is symmetric for a homosequence chain. Surprisingly, even for a homosequence, one can notice that the extension in hydrogen bonds is more stretched at the pulling end consists of thymine than the end consists of adenine in the atomistic simulations. The distribution of extension in covalent bonds along the chain also shows the asymmetry. One can observe that the bonds near the pulling end (5'-end) are more stretched and gradually decreases as one approaches the other end (i.e., the 3'-end).

### III. COARSE-GRAINED DESCRIPTION OF DNA RUPTURE

One of the possible reasons for such a discrepancy in theoretical models [14–16] is that they incorporate the same elasticity for the both strands. In recent years, there are considerable studies [28, 30–34] on the nature of the elasticity of ssDNA strands. For example, the force-extension

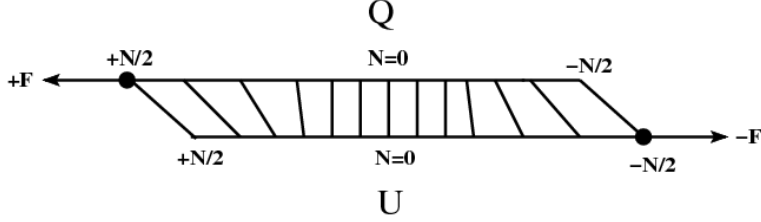


FIG. 4: Schematic representation of dsDNA under a shear force applied at the opposite ends ( $5' - 5'$  or  $3' - 3'$ ).

curves of ssDNA (or RNA) consisting of similar type of nucleotides show the striking differences [30, 31]. It was found that the poly(T) (or poly U) show the entropic response whereas poly(A) show the plateaus arising due to the base stacking. These studies provide unequivocal support for the use of different elastic constants for complementary strands (say adenine and thymine) in the model.

In view of this, we now use the coarse-grained description [3, 36–39] of the flexible polymer chain to model a dsDNA, which allows us to study a system of comparatively larger size. A chain in the model consists of bead units connected by effective bonds characterized by the stiff springs (Fig. 4). Each effective bond consists of several chemical bonds (*e.g.* sugar phosphate etc. ). A Lennard-Jones (LJ) potential is used to model the base pairing interaction between complimentary nucleotides. The energy of the model system is given by [36–38]

$$\begin{aligned}
 E = & \sum_{l=1}^2 \sum_{j=1}^N k^{(l)} (\mathbf{r}_{j+1,j}^{(l)} - d_0)^2 + \sum_{l=1}^2 \sum_{i=1}^{N-2} \sum_{j>i+1}^N 4 \left( \frac{C}{|\mathbf{r}_{i,j}^{(l)}|^{12}} \right) \\
 & + \sum_{i=1}^N \sum_{j=1}^N 4 \left( \frac{C}{(|\mathbf{r}_i^{(1)} - \mathbf{r}_j^{(2)}|)^{12}} - \frac{A}{(|\mathbf{r}_i^{(1)} - \mathbf{r}_j^{(2)}|)^6} \delta_{ij} \right), \quad (2)
 \end{aligned}$$

where  $N$  is the number of beads in each strand.  $\mathbf{r}_i^{(l)}$  represents the position of  $i^{th}$  bead on  $l^{th}$  strand. In present case,  $l = 1(2)$  corresponds to first (complimentary) strand of dsDNA. The distance between intra-strand beads,  $\mathbf{r}_{i,j}^{(l)}$ , is defined as  $|\mathbf{r}_i^{(l)} - \mathbf{r}_j^{(l)}|$ . The simplest approach to include semi-microscopic effects of nucleotides is to include different elastic constants as discussed above. The harmonic (first) term with spring constant  $k^l$  ( $k^1 = Q = 100$  &  $k^{(2)} = U = 60$ ) couples the adjacent beads along the two strands. Second term takes care of excluded volume effect *i.e.*

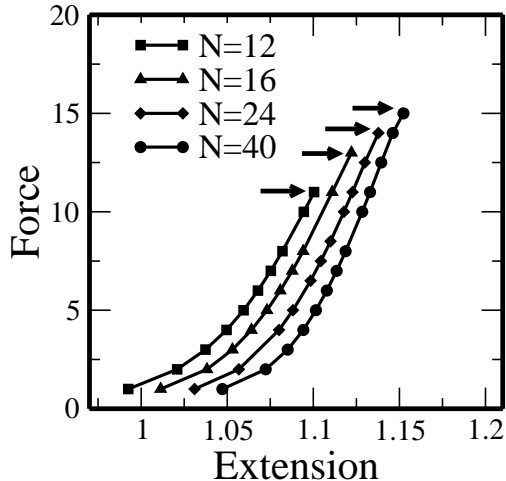


FIG. 5: Force *vs* extension curves for different lengths in the constant force ensemble. Arrows indicate the maximum force, where native contacts approaches to zero and two chains are separated. For the sake of comparison, we have normalized the extension by its chain length.

two beads can not occupy the same space [40]. The third term, described by Lennard-Jones (LJ) potential, takes care of the mutual interaction between two strands. The first term of LJ potential (same as second term of Eq.2) will not allow the overlap of two strands. Here, we set  $C = 1$  and  $A = 1$ . The second term of LJ potential corresponds to the base-pairing between two strands. The base-pairing interaction is restricted to the native contacts ( $\delta_{ij} = 1$ ) only *i.e.*  $i^{th}$  base of  $1^{st}$  strand forms pair with the  $i^{th}$  base of  $2^{nd}$  strand only as shown in Fig. 4, which is similar to the G $\bar{o}$  model [41]. The parameter  $d_0 (= 1.12)$  corresponds to the equilibrium distance in the harmonic potential, which is close to the equilibrium position of the LJ potential. In Eq. 2, we use dimensionless distances and energy parameters [35]. The major advantage of this model is that the ground state conformation is known. Therefore, equilibration is not an issue here, if one wants to study the dynamics under the applied force at low  $T$  [36]. The equation of motion is obtained from the following Langevin equation [17, 18, 36, 38]

$$m \frac{d^2 \mathbf{r}}{dt^2} = -\zeta \frac{d\mathbf{r}}{dt} + \mathbf{F}_c(\mathbf{t}) + \Gamma(t), \quad (3)$$

where  $m(= 1)$  and  $\zeta(= 0.4)$  are the mass of a bead and the friction coefficient, respectively. Here,  $F_c$  is defined as  $-\frac{dE}{dx}$  and the random force  $\Gamma$  is a white noise [18], i.e.,  $\langle \Gamma(t)\Gamma(t') \rangle = 2\zeta T\delta(t-t')$ , which ensures that the temperature of the system remains constant during the simulation for a given  $f$ . The 6<sup>th</sup> order predictor-corrector algorithm with time step  $\delta t=0.025$  [18] has been used to integrate the equation of motion. These results are averaged over many trajectories. The equilibration has been checked by monitoring the stability of data against at least ten times longer run. We have used  $2 \times 10^9$  time steps out of which first  $5 \times 10^8$  steps are not taken in the averaging.

In the constant force ensemble, we add an energy  $-\mathbf{f}\cdot\mathbf{x}$  to the total energy of the system given by Eq. 2, where  $\mathbf{x}$  is the extension along the applied force direction. The force-extension ( $f-x$ ) curve is shown in Fig. 5 for different lengths. The  $f-x$  curve shows the entropic response at low forces and remains qualitatively similar to the one seen in experiments. It may be noted that in the ladder model such response is missing as system remains in the stretched state. The rupture force is defined as a maximum force, where all the native contacts (*i.e.* number of intact base-pairs) suddenly goes to zero. The variation of the rupture force as a function of length of the chain for the low temperature ( $T = 0.06$ ) is shown in Fig. 6. One can notice that the rupture force approaches to an asymptotic value as length of the chain increases and is consistent with the experiment [10].

In Figs. 7 a, b, c & d, we show the distributions of extension in hydrogen bonds ( $\Delta_h$ ) along the chain for four different lengths. It may be noted that for the  $k^1 = k^2$  (or  $Q = U$ ), the distributions are symmetric [16]. However, for  $k^1 \neq k^2$  (or  $Q \neq U$ ), the distribution is asymmetric, which is consistent with the atomistic simulations presented in Sec. II. The characteristic de Gennes length for the present simulation appears to be approximately 8 bases, whose precise value is unknown. From this plot, one can observe that the hydrogen bonds near the extreme ends (up to  $\approx 8$  bases) get stretched, while the bases in the middle above the de Gennes length ( $\approx 8$  to 30 bases) remain unstretched indicating that the differential shearing force approaches to zero in this region. In Figs. 8 a, b, c & d, we show the variation of extension in the covalent bonds (back bone) along the chain. We observe similar asymmetry in the extension of covalent bonds for all lengths. The curve has three distinctively different regions. It shows that bonds near the pulling end (say 5'-end) are stretched more and gradually decrease. After the de Gennes length, they saturate and remain

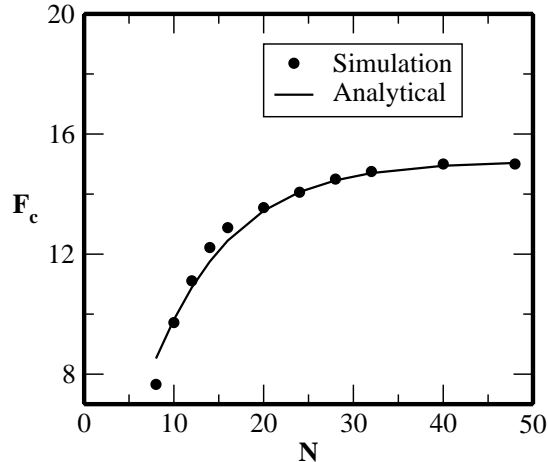


FIG. 6: The variation of rupture force with chain length. The solid line corresponds to a fit of Eq.5 with  $f_1 = 1$  and  $\chi \approx 0.118$ . Solid circles represent the value obtained through the simulation. A nice agreement with the theoretical prediction (Eq. 5) is apparent from the plot.

almost the same. However, when one approaches the other end (i.e. 3'-end), there is a change in the slope and the extension is quite less compare to the middle one. This is because of the fact that the 3'-end of first strand is near to the 5'-end of the other chain, where a similar force is also applied in the opposite direction. Since, the dsDNA is in the zipped state, the applied force at 5'-end of one strand also pulls the other strand along the opposite direction, which causes a relatively slower increase. Needless to mention that this increase also approaches to a constant value indicating that the differential shearing force also vanishes after the de Gennes length.

#### IV. DNA RUPTURE: ANALYTICAL SOLUTION

In order to get the precise value of de Geness length and critical rupture force, we consider the ladder model of DNA [14]. The semi-microscopic details *e.g.* inter and intra-strand stacking interactions, which give rise helecoidal structure, effect of pulling at 3' - 3' and 5' - 5' and heterogeneity in the sequence have not been included in the model. However, the covalent bonds of two strands (say made up of adenine (A) and thymine (T)) have been modeled by harmonic potentials with

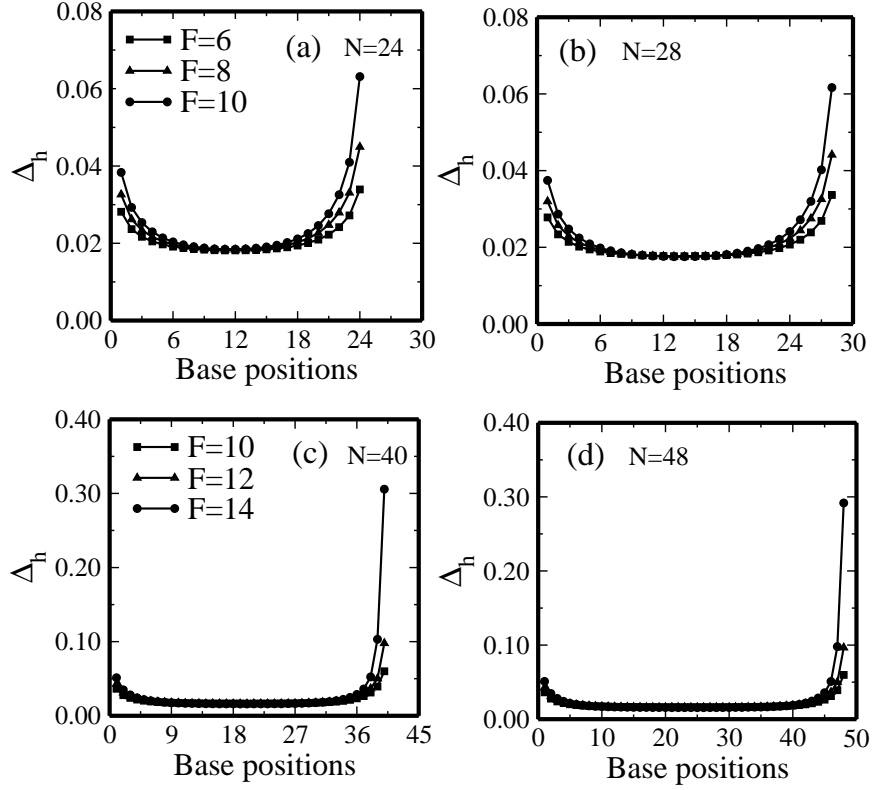


FIG. 7: Figs a,b,c & d show the variation of extension in hydrogen bond length ( $\Delta_h$ ) along the chain for the different length  $N=24, 28, 40$  and  $48$  respectively. It is obvious from these plots that the extension in hydrogen bonds for each length is asymmetric. It is because, both strands have different elastic constants ( $k^1 \neq k^2$ ). One can see that the elongation at the end of a strand having low elastic constant (where the force is applied) is much more than the middle one, where the differential force approaches to zero.

different spring constants ( $Q \neq U$ ). The base-pairing interaction for homosequence DNA is also modeled by the harmonic potential with the spring constant  $R$ . We apply the shear force on two strands as shown in Fig. 4. Let the displacements of the upper strand (say made up of A with large spring constant  $Q$ ) be  $u_n$  and lower strand (made up of thymine with smaller spring constant  $U$ ) be  $v_n$  for the  $n^{\text{th}}$  base-pair in a DNA chain of length  $N$  base-pairs. The Hamiltonian for the chain can be expressed as [14]

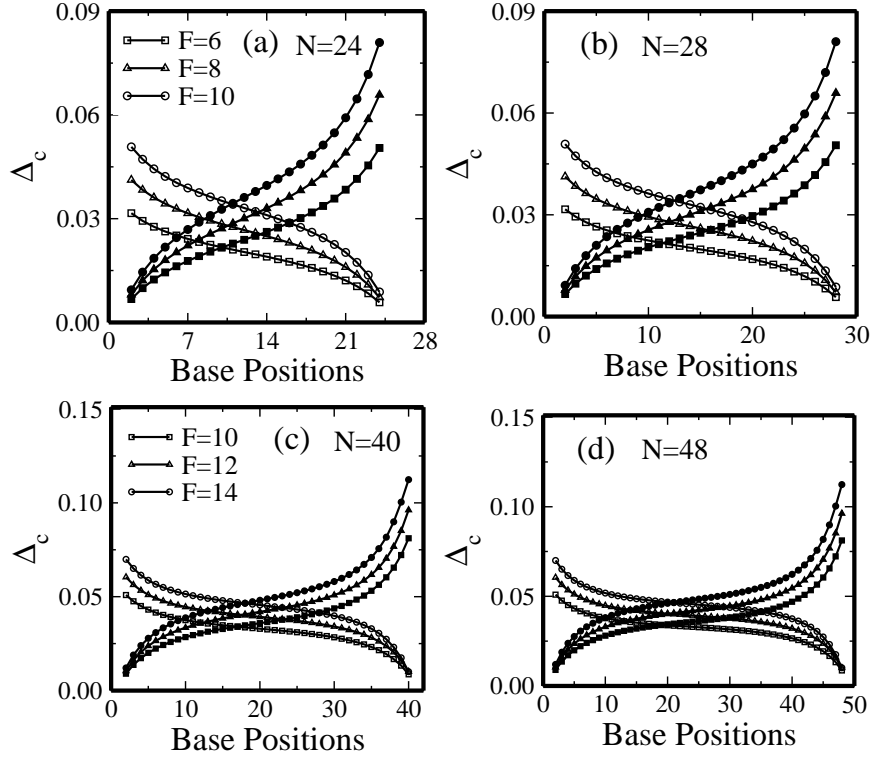


FIG. 8: Figs a,b,c & d show the variation in extension of covalent bond length ( $\Delta_c$ ) along the chain for the different chain length  $N=24, 28, 40$  and  $48$ , respectively. The asymmetry in the extension of covalent bonds is apparent from these plots for each length. Open and filled symbols correspond to one strand and its complementary strand, respectively. The larger extension in bond length corresponds to the end of a strand having low elastic constant (where the force is applied), whereas the minimum extension in bond length corresponds that the force is applied at the other end of the complimentary strand having larger elastic constant. The differential force here also approaches to zero.

$$\begin{aligned}
H = & \sum_{n=-\frac{N}{2}}^{\infty} \frac{1}{2} Q(u_n - u_{n+1})^2 + \sum_{n=-\infty}^{\frac{N}{2}} \frac{1}{2} U(v_n - v_{n+1})^2 \\
& + \sum_{n=-\frac{N}{2}}^{\frac{N}{2}} \frac{1}{2} R(v_n - u_n)^2.
\end{aligned} \tag{4}$$

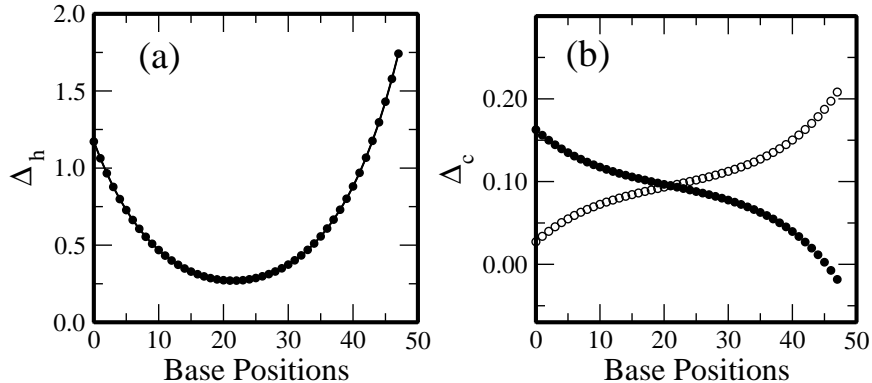


FIG. 9: Fig (a) shows the variation of extension in hydrogen bond length ( $\Delta_h$ ) along the chain with base position. (b) Variation in extension of covalent bond length ( $\Delta_c$ ) along the chain length. Here, open and filled symbols correspond to one strand and its complementary strand, respectively.

Following Ref. [14], we evaluate the expression for de Gennes characteristic length  $\chi^2 = \frac{R(Q+U)}{QU}$ , when the elasticity of two strands are not same. Here,  $R \ll Q$  and  $U$ . The relation between the rupture force  $F_C$  and the chain length for this model is given by (see Appendix A)

$$\frac{F_c}{f_1} = \frac{2 \tanh(\chi N/2)}{\chi \left(1 + \frac{(Q-U)}{(Q+U)} \left[ \frac{\chi + \tanh(\chi N/2)}{1 + \chi \tanh(\chi N/2)} \right] \tanh(\chi N/2) \right)}. \quad (5)$$

Though, the equation looks complicated, but it has only two free parameters  $Q$  and  $U$ , whose value can be obtained experimentally. For a long chain, Eq. 5 reduces to

$$\frac{F_c}{f_1} \approx \frac{Q+U}{\chi Q}. \quad (6)$$

For  $Q = U$ , Eq. 5 reduces to the Eq. 1 as proposed by de Gennes [14]. In Fig. 9, we depict the distribution of extension in hydrogen bonds and covalent bonds with base position at critical force  $F_c$  (see Appendix A). These distribution are qualitatively similar to the one obtained in the atomistic simulations (Sec. II) and the coarse-grained simulations (Sec. III).

The de Gennes characteristic length for the L-J potential can be obtained by expanding the L-J potential given in Eq.2 around its equilibrium value and equating the coefficient of second term of its expansion with harmonic spring. For the present model it is estimated to be  $\approx 0.118$ . Substituting values of  $f_1 (= 1)$  and the above mentioned value of  $\chi$  in Eq. 5, one can obtain the

value of  $F_c$  for a given length of dsDNA. In Fig. 6, we also show the behavior of the rupture force as a function of DNA length obtained from Eq. 5. One can notice a nice agreement with simulations and analytical result obtained here.

## V. CONCLUSIONS

In this paper, we have performed atomistic simulations to study the effect of shear force on the rupture of dsDNA. In contrast to the previous studies [14–16], here the distribution of extension in hydrogen and covalent bonds show the asymmetry. This asymmetry arises because of different elastic constants of the strands. Inclusion of different elastic constants in the description of the coarse-grained model gives qualitatively similar behavior as seen in the atomistic simulations. For a short chain, we find that the rupture force increases linearly and saturates for a longer chain, which is consistent with the experiment and earlier studies [10, 16]. The distribution of hydrogen bonds show that differential force penetrates up to the de Gennes characteristic length. Using the ladder model of DNA, we have obtained the analytical expression for the de Gennes characteristic length and rupture force for the chains whose complimentary strands have different elastic constants. These values are in very good agreement with the coarse-grained simulations. By setting  $k^1 = k^2$  (or  $Q = U$ ), the expression reduces to the de Gennes expression Eq. 1 [14].

It is possible to extend the approach developed here in understanding many intramolecular processes such as microsatellites formation, bulge loop propagation in repetitive sequences which exhibits complex dynamics and a distinct biological function. Our studies may provide the mechanism involved in ligand receptor binding in cell’s tissue at molecular level and DNA protein interactions. An all atoms simulation can provide the life time of these interactions, which can be verified by the time resolved spectroscopy. One would also able to know whether all interactions contribute at the same moment or have different life times.

We thank Garima Mishra, M. Santosh and P. K. Maiti for many helpful discussions on the subject. We also thank P. K. Maiti for providing us the constant force routine for the atomistic simulations. Financial supports from the Department of Science and Technology, Council of Scientific and Industrial Research, New Delhi are gratefully acknowledged. The generous computer

support from IUAC New Delhi is also acknowledged by the authors. One of the authors (SK) would like to acknowledge the Sonderforschungsbereich/Transregio SFB/TRR 102 Halle-Leipzig *Polymers under Multiple Constraints: Restricted and Controlled Molecular Order and Mobility* for his visit at Institute of Physics, University of Leipzig, Germany, where a part of the work is carried out.

## Appendix A

Under the application of shear force, Eq. 4 gives the equilibrium condition for the upper strand as

$$\frac{\partial H}{\partial u_n} = Q(u_{n+1} - 2u_n + u_{n-1}) + R(v_n - u_n) = 0 \quad (\text{A1})$$

and similarly for the lower strand,

$$\frac{\partial H}{\partial v_n} = U(v_{n+1} - 2v_n + v_{n-1}) + R(u_n - v_n) = 0. \quad (\text{A2})$$

For large N, Eq.A.1 and Eq.A.2 can be expressed in continuum limit of  $n$  as

$$Q \frac{d^2 u_n}{dn^2} + R(v_n - u_n) = 0 \quad (\text{A3})$$

$$U \frac{d^2 v_n}{dn^2} - R(v_n - u_n) = 0. \quad (\text{A4})$$

By adding Eqs. A.3 and A.4, we get

$$Q \frac{d^2 u_n}{dn^2} + U \frac{d^2 v_n}{dn^2} = 0. \quad (\text{A5})$$

Thus from the solution of Eq. A.5 as the total tension constant, we obtain the following condition:

$$Qu_n + Uv_n = nF. \quad (\text{A6})$$

On multiplying Eq. A.3 by U and Eq. A.4 by Q, and subtracting we obtain,

$$\frac{d^2 \delta_n}{dn^2} - \frac{R(Q+U)}{QU} \delta_n = 0, \quad (\text{A7})$$

where,  $\delta_n = v_n - u_n$ . This is a simple second order differential equation whose solution is of the form:

$$\delta_n = \delta_0 \cosh(\chi n) + A \sinh(\chi n), \quad (\text{A8})$$

where  $\chi^2 = \frac{R(Q+U)}{QU}$  and A is an arbitrary constant of integration. From Eqs. A.6, A.7 and A.8, we get

$$\begin{aligned} v_n &= \frac{nF}{Q+U} + \frac{Q}{Q+U} \delta_0 \cosh(\chi n) \\ &+ \frac{AQ}{Q+U} \sinh(\chi n) \end{aligned} \quad (\text{A9})$$

$$\begin{aligned} u_n &= \frac{nF}{Q+U} - \frac{U}{Q+U} \delta_0 \cosh(\chi n) \\ &- \frac{AU}{Q+U} \sinh(\chi n) \end{aligned} \quad (\text{A10})$$

The force at both the ends ( $\frac{N}{2}$  and  $-\frac{N}{2}$ ) of the strand must be balanced. Thus,

$$F = U(v_{\frac{N}{2}} - v_{\frac{N}{2}-1}) + R(v_{\frac{N}{2}} - u_{\frac{N}{2}}) \quad (\text{A11})$$

$$-F = Q(u_{-\frac{N}{2}} - u_{-(\frac{N}{2}-1)}) + R(u_{-\frac{N}{2}} - v_{-\frac{N}{2}}), \quad (\text{A12})$$

which gives a relation between A and  $\delta_0$  as

$$A = \delta_0 \frac{(Q-U) (\sinh(\chi N/2) + \chi \cosh(\chi N/2))}{(Q+U) (\cosh(\chi N/2) + \chi \sinh(\chi N/2))} \quad (\text{A13})$$

The overall force acting on the base-pairs of the dsDNA can be calculated as the sum of restoring forces on the base-pairs,

$$F = \sum_{n=-\frac{N}{2}}^{\frac{N}{2}} R\delta_n = \int_{-N/2}^{N/2} R\delta_n dn = \frac{2R\delta_0 \sinh(\chi N/2)}{\chi} \quad (\text{A14})$$

The rupture will take at critical force  $F_c$  from the end ( $n = N/2$ ), because the end base-pair ( $N/2$ ) will have maximum elongation. If the force required to break a base-pair is  $f_1$ , then

$$\begin{aligned} f_1 &= R\delta_0 [\cosh(\chi N/2) + \\ &+ \frac{(Q-U)}{(Q+U)} \left[ \frac{\sinh(\chi N/2) + \chi \cosh(\chi N/2)}{\cosh(\chi N/2) + \chi \sinh(\chi N/2)} \right] \sinh(\chi N/2)] \end{aligned} \quad (\text{A15})$$

Dividing Eq. A. 14 by A.15, we get a relation between the rupture force  $F_C$  and the  $f_1$

$$\frac{F_c}{f_1} = \frac{2 \tanh(\chi N/2)}{\chi \left(1 + \frac{(Q-U)}{(Q+U)} \left[ \frac{\chi + \tanh(\chi N/2)}{1 + \chi \tanh(\chi N/2)} \right] \tanh(\chi N/2) \right)} \quad (\text{A16})$$

- 
- [1] B. Alberts, D. Bray, J. Lewis, M. Raff, K. Roberts and J. D. Watson, *Molecular Biology of the Cell*, (Garland Publishing: New York, 1994).
- [2] J. N. Israelachvili, *Intermolecular and Surface Forces* (Academic Press, London, 1992).
- [3] S. Kumar, M. S. Li, Phys. Rep. **486**, 1 (2010).
- [4] B. Essevaz-Roulet, U. Bockelmann, and F. Heslot, PNAS **94**, 11935 (1997).
- [5] U. Bockelmann, B. Essevaz-Roulet and F. Heslot, Phys. Rev. Lett. **79**, 4489 (1997).
- [6] G. U. Lee, L. A. Chrisey, and R. J. Colton, Science, **266**, 771 (1994).
- [7] T. Strunz, K. Oroszlan, R. Schäfer and H.J. Günterodt, PNAS **96**, 11277 (1999).
- [8] I. Schumakovitch, W. Grange, T. Strunz, P. Bertoncini, H-J. Güntherodt, M. Hegner, Biophys J. **82**, 517 (2002).
- [9] C. Danilowicz, Y. Kafri, R. S. Conroy, V. W. Coljee, J. Weeks, and M. Prentiss, Phys. Rev. Lett. **93**, 078101 (2004).
- [10] K. Hatch, C. Danilowicz, V. Coljee, and M. Prentiss, Phys. Rev. E **78** 011920 (2008).
- [11] C. Danilowicz, C. Limouse, K. Hatch, A. Conover, V. W. Coljee, N. Klecknerb and M. Prentiss, PNAS **106**, 13196 (2009).
- [12] F. Kueher, J. Morfill, R. A. Neher, K. Blank, and H. E. Gaub, Biophys. J **92**, 2491 (2007)
- [13] A. M. Naserian-Nik, M. Tahani and M. Karttunen, RSC Advances (2013) [DOI: 10.1039/C3ra23213a].
- [14] P. G. de Gennes, C. R. Acad. Sci.-Ser. IV- Phys. **2**, 1505 (2001).
- [15] B. Chakrabarti and D. Nelson, J. Phys. Chemi. B **113** 3831 (2009).
- [16] R. K. Mishra, G. Mishra, M. S. Li, and S. Kumar, Phys. Rev. E **84** 032903 (2011).
- [17] M. P. Allen, D. J. Tildesley, *Computer Simulations of Liquids* (Oxford Science, Oxford, UK, 1987).
- [18] D. Frenkel and B. Smit *Understanding Molecular Simulation* (Academic Press UK, 2002).
- [19] D. A. Case, T. A. Darden, T. E. Cheatham, III, C. L. Simmerling, J. Wang, R. E. Duke, R. Luo, M. Crowley, R. C. Walker, W. Zhang, K. M. Merz, B. Wang, S. Hayik, A. Roitberg, G. Seabra, I. Kolossvry, K.F. Wong, F. Paesani, J. Vanicek, X. Wu, S.R. Brozell, T. Steinbrecher, H. Gohlke, L. Yang, C. Tan, J. Mongan, V. Hornak, G. Cui, D.H. Mathews, M.G. Seetin, C. Sagui, V. Babin, and P.A. Kollman, (2008), AMBER 10 (University of California, San Francisco).

- [20] Y. Duan, C. Wu, S. Chowdhury, M. C. Lee, G. Xiong, W. Zhang, R. Yang, P. Cieplak, R. Luo, T. Lee, J. Caldwell, J. Wang, P. Kollman, *J. Comput. Chem.* **24**, 1999 (2003).
- [21] M. Santosh and P. K. Maiti, *J. Phys.: Condens. Matter* **21**, 034113 (2009).
- [22] We used the constant force routine developed by P. K. Maiti and his group.
- [23] T. Darden, D. York and L. Pedersen, *J. Chem. Phys.* **98**, 10089 (1993).
- [24] U. Essmann, L. Perera, M. L. Berkowitz, T. Darden, H. Lee, and L. G. Pedersen, *J. Chem. Phys.* **103**, 8577 (1995).
- [25] W. L. Jorgensen, J. Chandrasekhar, and J. D. Madura *J. Chem. Phys.* **79** (1983).
- [26] P. K. Maiti, T. A. Pascal, N. Vaidehi and W. A. Goddard III, *Nucleic Acids Res.* **32**, 6047 (2004).
- [27] P. K. Maiti and B. Bagchi, *Nano Lett.* **6**, 2478 (2006).
- [28] N. L. Goddard, G. Bonnet, O. Krichevsky, and A. Libchaber *Phys. Rev. Lett.* **85**, 2400 (2000).
- [29] W. Humphrey, A. Dalke, and K. Schulten, *J. Mol. Graphics*, **14** 33 (1996).
- [30] Y. Seol, G. M. Skinner, and K. Visscher *Phys. Rev. Lett.* **98**, 158103 (2007).
- [31] C. Ke, M. Humeniuk, H. S-Gracz, and P. E. Marszalek *Phys. Rev. Lett.* **99**, 018302 (2007).
- [32] G. Mishra, D. Giri, and S. Kumar *Phys. Rev. E* **79**, 031930 (2009).
- [33] K. Singh, S. K. Ghosh, S. Kumar and A. Sain *EPL*, **100**, 68004 (2012).
- [34] S. Kumar and G. Mishra *Soft Matter* **7**, 4595 (2011).
- [35] For melting the free energy per base is approximately -1.2 kcal/mol, which includes base pairing as well as stacking (inter and intra). However in rupture, we assume that there are breaking of hydrogen bonds (base pairing) only and stacking does not contribute significantly. For such a case if one takes free energy approximately -0.6 kcal/mol per base of the zipped conformation [16] and equate it with the ruptured state, it is possible to parametrize the rupture force also.
- [36] M. S. Li, M. Cieplak, *Phys. Rev E* **59**, 970 (1999).
- [37] M. Kouza, C-F. Chang, S. Hayryan, T-H. Yu, M. S. Li, T-H. Huang, C-K. Hu, *Biophys. J.* **89**, 3353 (2005).
- [38] M. S. Li, *Biophys. J.* **93**, 2644 (2007).
- [39] J. Schluttig, M. Bachmann and W. Janke, *J. Comput. Chem.* **29**, 2603 (2008); S. Kumar and Y. Singh, *J. Phys. A:Math & Gen* **26**, L987 (1993).
- [40] P. G de Gennes, *Scaling concepts in Polymer Physics*, (Cornell University press, Ithaca, 1979)
- [41] N. Gō and H. Abe, *Biopolymers* **20**, 991 (1981).
- [42] E. T. Kool, *Annu. Rev. Biophys. Biomol. Struct.* **30**, 1 (2001).